SICE Annual Conference 2010
August 18-21, 2010, The Grand Hotel, Taipei, Taiwan

The Stepping over an Obstacle for the Humanoid Robot with the Consideration of Dynamic Balance

Chih-Lyang Hwang, Han-Chen Wu, and Ming-Lung Lin

Department of Electrical Engineering, Tamkang University, 25137 Taiwan, R.O.C.

Abstract—This paper presented a fuzzy decentralized controller for a small size humanoid robot (HR) to stepping over the known obstacle and keeping balance when the force disturbance occurs. The proposed HR possessed 55 *cm* height, 3.7 *kg* weight, and 21 degree-of-freedom (DOF). This paper contains motion control, posture capture, and dynamic balance control. The first part designed a standard motion of stepping over the obstacle by human-machine interface. The second part set a posture captured sensors combining with two gyro sensors and one accelerometer. Based on SOPC (System on a Programmable Chip), it operated with parallel processing. This suggested sensors captured the responses of the pitch axis and roll axis during the stepping over the obstacle. On the other hand, the Kalman filter was applied to improve the measure accuracy. The fuzzy decentralized control (FDC) to keep the dynamic balance was then considered as the third part. During the steeping over the obstacle, the HR was punched by a standard hammer to verify the effectiveness of the proposed FDC. Finally, the corresponding experiments of steeping over obstacle with punched disturbance confirmed the suggested result.

Keywords: Humanoid robot, Stepping over the obstacle. Human-machine interface, Dynamic sensors and balance, Fuzzy decentralized control.

I. Introduction

There are many researches about autonomous humanoid robot [1]-[13]. Their corresponding topics are expressed as follows. In recent years, Loffler et al. [1] discussed sensors and control concept of a biped robot. A known forward operation for a specific task combined with the sensory reflex control for a humanoid robot was developed by Huang and Nakamura [2]. In addition, a stepping over obstacles with humanoid robot was discussed by Guan et al. [3]. It merely discussed the static balance. Harada et al [4] discussed a real-time planning of humanoid robot's gait for force-controlled manipulation. Neo et al. [5] discussed the whole-body motion generation integrating operator's intention and robot's autonomy in controlling humanoid robots. A new active visual for humanoid robot was discussed by Xu et al. [6]. Arechavaleta et al. [7] discussed an optimality principle governing human walking. Montesano et al. [8] demonstrated successful learning in the real world by having a humanoid robot interacting with objects. Two psychological scales, namely negative attitudes toward robots scale and robot anxiety scale, are defined. The subjects and a humanoid robot are engaged in simple interactions including scenes of meeting, greeting, self-disclosure, and physical contact [9]. Gait synthesis and sensory control of the stair climbing for a humanoid robot was discussed by Fu and Chen [10]. In addition, Kanda *et* al. [11] investigates the interactions between human and humanoid robots: Robovie and ASIMO. Yoshida et al. [12] planned a 3-D collision-free dynamic robotic motion through iterative reshaping. Recently, t**he paper [13] presents three feedback controllers that achieve an asymptotically stable, periodic, and fast walking gait for a 3-D bipedal robot consisting of a torso, revolute knees, and passive point feet. According to the above analysis, h**umanoid robots are expected to take an important role in assisting activity in human daily environments owing to their flexibility and friendly appearance.

There have many factors affecting the stepping over an obstacle of a humanoid robot (HR), e.g., the height and width of the obstacle, the design of servomachanisim, the strategy for dynamic balance [14], [15]. In this paper, the dynamic balance of the stepping over an obstacle is addressed. It is different from the previous paper [3], which merely discussed a static balance. It implies that the walking velocity of the HR in the paper [3] should not too fast to preserve its stability for stepping over an obstacle. In the beginning, the dynamic sensing systems, i.e., two sets of pressure sensors and three single-axis gyros, are calibrated. During a stable stepping over an obstacle, these two sets of pressure sensors and three single-axis gyros are respectively employed to obtain the response of the center of pressure (COP) and the posture of the HR [10], [16]-[18]. The COP of the HR inludes two catgories: one is single support phase (SSP), the other is double support phase (DSP). Based on the analysis of the stepping over an obstacle, six important steps are described as follows: (i) two feet are initially parallel (DSP), (ii) left foot lifts to step over an obstacle (SSP), (iii) left foot reaches the ground (DSP), (iv) the posture of the upper body of the HR is adjusted to change the center of gravity of the HR to the left foot (DSP), (v) right foot lifts to finsih the task of the steppng over an obstacle, and (vi) back to the posture of step (i) [3], [14], [15]. During steps 2~6, the arm must adjust according to the principle that different leg and different arm are asymmetric. For example, if the left (right) leg is in front of the right (left) foot, left and right (right and left) arms must swing bacward and forward, respectively.

After the anaysis of the response, the suitable path for the stepping over an obstacle is planned such that three reference inputs for the fuzzy decentralized balance control (FDBC) are developed [19]. The reasons to use the FDBC are that the dynamics of the HR is complex, coupled, and highly nonlinear, and that the balance control possesses the unstable feature. If the tilt moment does not adjust in time, the HR will fall down the ground. In this situation, three sing-axis gyros are employed to measure the posture of the HR for improving the dynamic balance of the stepping over an obstacle. Certainly, the estimated posture must be calibrated before it is used for the feedback control. According to

The authors would like to appreciate the financial support from National Council of Science of R.O.C. with Grant No. NSC 98-2218-E-032 -002.

PR0001/10/0000-2260 ¥400

these two signals, two reference inputs with two DOF are planned for the balance control of the HR. Then the dynamic balance of HR is guaranteed by four pairs of fuzzy decentralized balance controls for two DOF of ankle and two DOF of waist for each leg as it is either in SSP or DSP. Furthermore, human-HR interface for the motion control of the nominal condition of the stepping over an obstacle is obtained. No inverse kinematics is required for FDBC. At first, the standing HR in the presence of disturbance with (or without) the consideration of the dynamic balance is compared to verify the effectiveness of the proposed control method. Then the corresponding experiments of the stepping over an obstacle on the flat and slope grounds in the face of disturbance are investigated.

II. Experimental Setup

The photograph of the HR is depicted in the Fig. 2(a), which possesses 21 degree-of-freedom (DOF) with the weight of 5 kg and the height of 50 *cm*. The specifications of the HR are described as follows: The servomotors are the Model No. of AX-12, RX-28, and RX-64 from Robotis Co. Based on the weight and torque of servomotor and the required torque for the motion of HR, the arm and leg, and knee of the HR respectively use the model AX-12, RX-28 and RX-64. The HR has 6 DOF for each leg, 4 DOF for each arm, 1 DOF for the body (or 3 DOF for the body including 2 DOF common with two legs). The corresponding DOF is expressed in Fig. 2(b). One of dominant feature of the servomotor from Robotis Co. is its command by the peripheries of RS-485 and TTL UART, which is different from the PWM for the other servomotor.

The embedded system RB-100 contains four kind of UART: RS-232, RS-485, TTL full duplex, and TTL half duplex, and it is described as follows: dimension 96x56 mm, weight 40g, CPU DM&P Vortex86DX, 256MB DDR2, power consumption +5V @400mA, input DC voltage 6~24V. The operating system of embedded system RB-100: DOS, Windows 98/ME, Windows XP/ XP Embedded, Windows Embedded CE, and Windows Embedded Standard Linux. An integrated circuit (see Fig. 2(c)) is also designed for the reduction of connection wire. In addition, the position, temperature and voltage can be transmitted through it to design an intelligent robot. In order to operate the HR, we have designed a human-interface (see Fig.3) to give position and velocity commands for every motor. The command can simultaneously or sequentially drive a set of specific motors.

The NIOS processer contain the core chip of EP2C35 which made by Altera Co. This chip contains 33216 logic gate, 484 Kbit memory and 35 hardware multipliers. The NIOS microcontroller is base on SOPC (System on a Programmable Chip). We design the SPI module with the hardware description language of Verilog, in Fig.4 is the SPI module of accelerometer, Fig.5 is the SPI module of gyro. The NIOS microcontroller takes the operation of sensor data capture with parallel processing. In addition, the active vision system in Fig. 2(c) does not consider in this paper. Hence, the corresponding details are omitted.

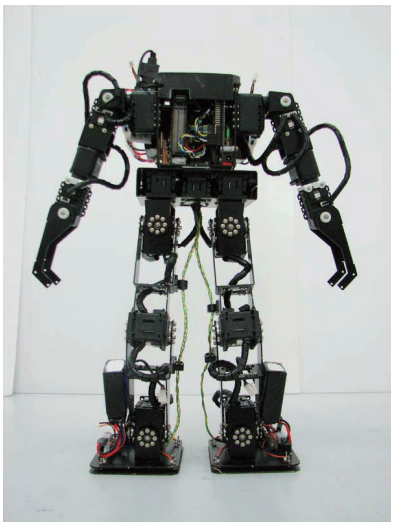

(a) Photograph of the HR.

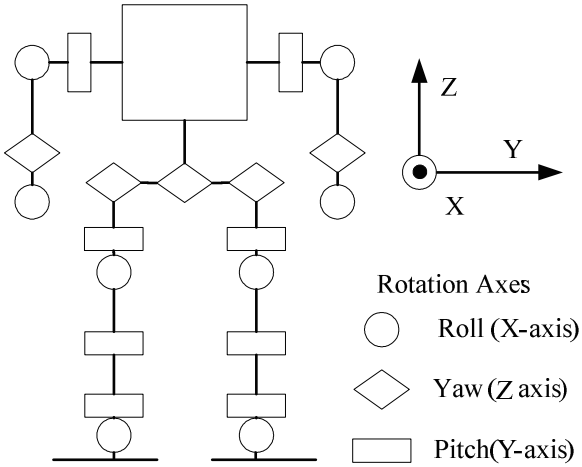

(b) DOF of the HR.

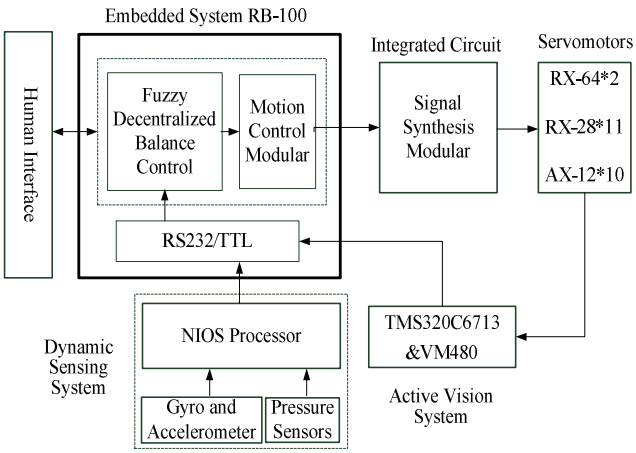

(c) Block diagram of the HR.

Fig. 2. Architecture of an HR.

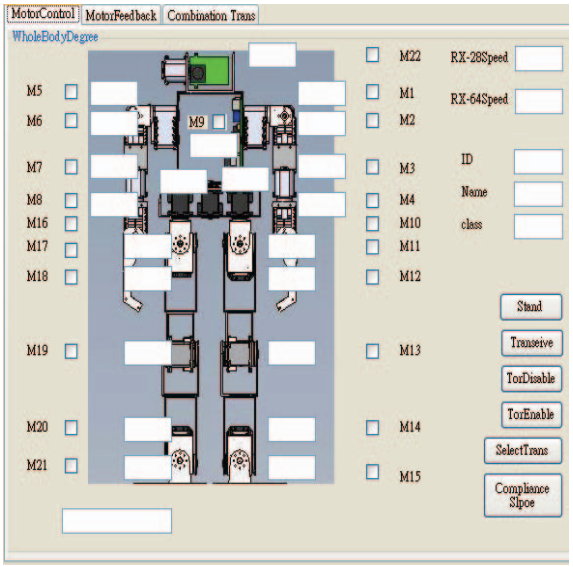

Fig. 3 A human-interface for the operation of HR.

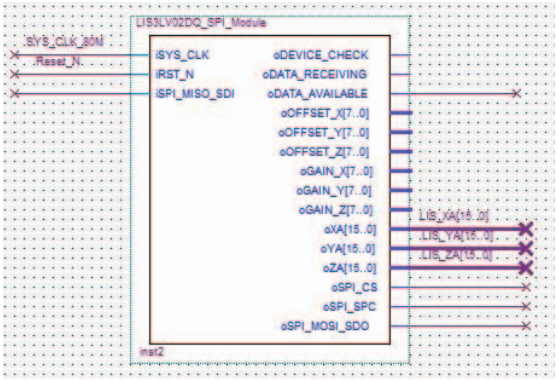

Fig. 4. The SPI module of accelerometer.

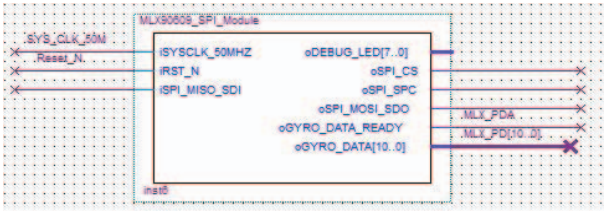

Fig. 5. The SPI module of gyro.

III. Dynamical Sensors and Posture Detection

The purpose of posture detection is to obtain the angular position of roll-axis and pitch-axis. This dynamic sensing system is developed by 3 sensors: a three-axis accelerometer in Fig.6 and two single-axis gyros in Fig. 7.The corresponding coordinates are respectively depicted in Fig. 6 and Fig. 7. It is known that these two kinds of sensor have their own shortages in accumulated error and measurement error. If only gyro sensor is applied to detect the angular position, even the HR does not move its response results in the drifted feature (e.g., Fig.8). On the other hand, only accelerometer is employed to detect the angular position, even the HR does not move, when the horizontal moving occur, the acceleration is possibly rotated (e.g., Fig.9).

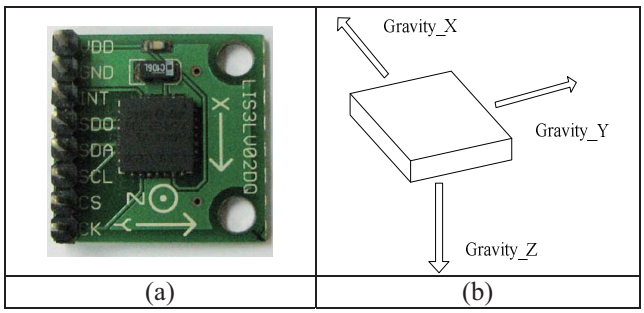

Fig. 6. Three-axes accelerometer.

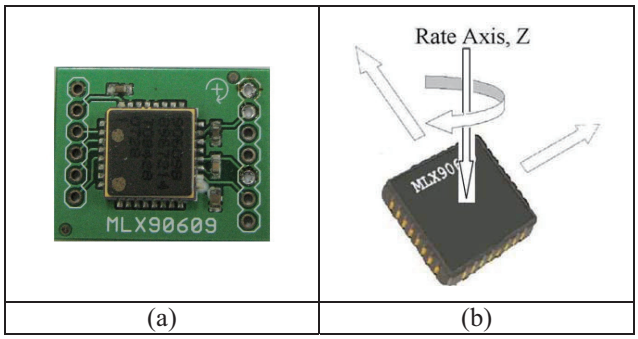

Fig. 7. One-axis gyro.

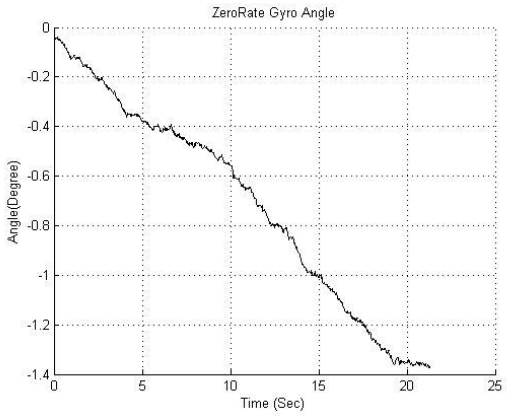

Fig. 8 The drift of gyro with zero rate.

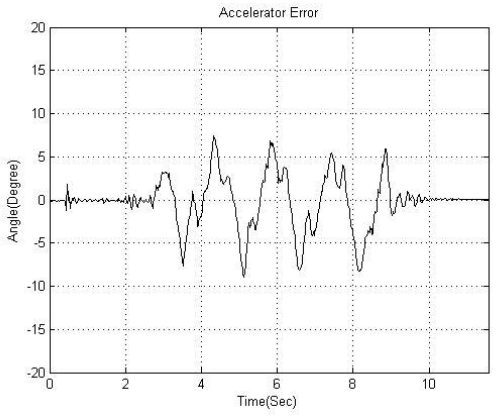

Fig. 9. The acceleration error caused by horizontal motion.

To eliminate these errors, a Kalman filter is employed to pre-process the sensor data. The purpose of Kalman filter is to use measurements that are observed over time that contain noise (random variations) and other inaccuracies, and produce values that tend to be closer to the true values of the measurements and their

associated calculated values. The Kalman filter is a recursive estimator. It contains two essential parts: predict and update. There are two variables of the state of the filter:

(i) There are two formulas in the predict part:

$$\hat{X}_{k|k-1} = F_k \hat{X}_{k-1|k-1} + B_k U_k \quad (1)$$

$$P_{k|k-1} = F_k P_{k-1|k-1} F_k^T + Q_k \quad (2)$$

where $\hat{X}_{k|k}$ and $P_{k|k}$ respectively denote the estimated state of the system and the error covariance matrix using the signal up to and including time-step k, Q_k is the covariance of the system noise, F_k and B_k are the state transition and control gain matrices at time-step k.

(ii) There are five formulas in the update part:

$$\tilde{Y}_k = Z_k - H_k \hat{X}_{k|k-1} \quad (3)$$

$$S_k = H_k P_{k|k-1} H_k^T + R_k \quad (4)$$

$$K_k = P_{k|k-1} H_k^T S_k^{-1} \quad (5)$$

$$\hat{X}_{k|k} = \hat{X}_{k|k-1} + K_k \tilde{Y}_k \quad (6)$$

$$P_{k|k} = (I - K_k H_k) P_{k|k-1}. \quad (7)$$

where Z_k is the observed (or measured) signal, H_k is the observation model, R_k is the covariance of the observation noise, K_k is the Kalman filter gain.

In the predict part, the variables are defined as follows:

$$X_{k-1|k-1} = \begin{bmatrix} \theta_{k-1} \\ G_{bias,k-1} \end{bmatrix}$$

$$P_{k-1|k-1} = \begin{bmatrix} P_{00,k-1} & P_{01,k-1} \\ P_{10,k-1} & P_{11,k-1} \end{bmatrix}$$

$$Q_k = \begin{bmatrix} Q_{00} & 0 \\ 0 & Q_{11} \end{bmatrix}$$

$$F_k = \begin{bmatrix} 1 & -\Delta t \\ 0 & 1 \end{bmatrix}, \quad B_k = \begin{bmatrix} \Delta t & 0 \\ 0 & 0 \end{bmatrix}, \quad U_k = \begin{bmatrix} \omega \\ 0 \end{bmatrix}$$

where θ_{k-1} is the Kalman degree of time k-1, $G_{bias,k-1}$ is the gyro bias of time k-1, Δt is sampling time, and ω is the angular velocity from the gyro. Hence,

$$X_{k|k-1} = F_k X_{k-1|k-1} + B_k U_k = \begin{bmatrix} \theta_{k-1} + (\omega - G_{Bias,k-1})\Delta t \\ G_{Bias,k-1} \end{bmatrix}$$

$$P_{k|k-1} = F_k P_{k-1|k-1} F_k^T + Q_k$$

$$= \begin{bmatrix} P_{00,k-1} - \Delta t(P_{10,k-1} + P_{01,k-1} - P_{11,k-1}\Delta t) + Q_{00} & P_{01,k-1} - P_{11,k-1}\Delta t \\ P_{10,k-1} - P_{11,k-1}\Delta t & P_{11,k-1} + Q_{11} \end{bmatrix}.$$

In the update part, the variables are defined as follows:

$$P_{k|k-1} = \begin{bmatrix} P_{00,k} & P_{01,k} \\ P_{10,k} & P_{11,k} \end{bmatrix}, \quad R_k = [r_k], \quad H_k = [1 \quad 0],$$

and $K_k = \begin{bmatrix} K_0 \\ K_1 \end{bmatrix}$.

Hence,

$$Y_k = Z_k - H_k X_{k|k-1} = \theta_m - [1 \quad 0] \begin{bmatrix} \theta_k \\ G_{bias,k-1} \end{bmatrix} = \theta_m - \theta_k$$

$$S_k = H_k P_{k|k-1} H_k^T + R_k = P_{00,k} + r_k$$

$$K_k = P_{k|k-1} H_k^T S_k^{-1} = \begin{bmatrix} P_{00,k} \\ P_{10,k} \end{bmatrix} S_k^{-1}$$

$$X_{k|k} = X_{k|k-1} + K_k Y_k = \begin{bmatrix} \theta_k + K_0 Y_k \\ G_{bias,k} + K_1 Y_k \end{bmatrix}$$

$$P_{k|k} = (I - K_k H_k) P_{k|k-1}$$

$$= \begin{bmatrix} P_{00,k} - P_{00,k} K_0 & P_{01,k} - P_{01,k} K_0 \\ P_{10,k} - P_{00,k} K_1 & P_{11,k} - P_{01,k} K_1 \end{bmatrix}$$

where θ_m is the degree from the accelerometer. The parameters and initial values of the experiment are set as follows:

$$X_{k-1|k-1} = \begin{bmatrix} 0 \\ 148.008270 \end{bmatrix}, \quad \Delta t = \frac{1}{820} = 0.0012195121$$

$$Q_k = \begin{bmatrix} 0.000000003 & 0 \\ 0 & 0.0000007 \end{bmatrix}, \quad R_k = [0.525].$$

In summary, the operate procedure of Kalman filter is shown in Fig.10.

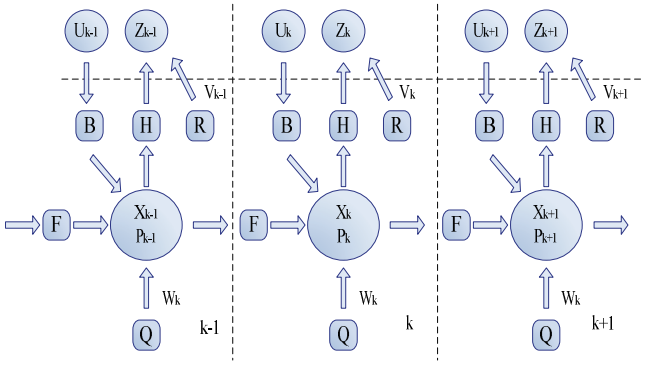

Fig. 10 The operation procedure of Kalman filter.

To test and verify the accuracy of posture detection, three tests of motion based on the basic motions of HR (i.e., Fig.11) are progressed. The all sensors is set upon a motor and rotates in roll-axis only. The first test is the oscillation in 30 degrees with a specific frequency (see Fig.12), the second test is the rotation at will (see Fig.13), the third test is horizontal motion with a specific velocity (see Fig.14). At the mean while, the motor feedback is also recorded. The results of all three tests of Figs. 12~14 as compared with the result of Kalman filter are shown in Fig.15. The average error between measured rotation and motor feedback is 0.7395 degree.

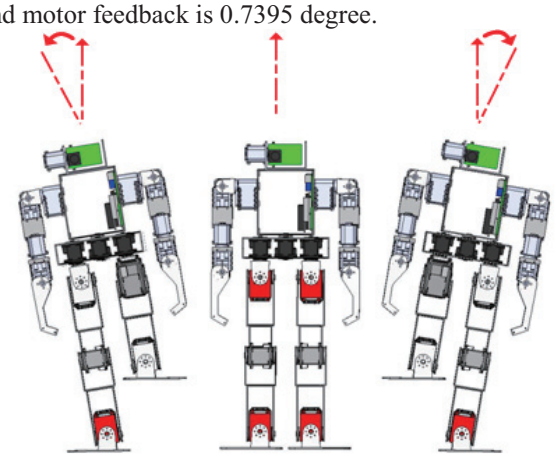

Fig. 11. The basic motions of HR.

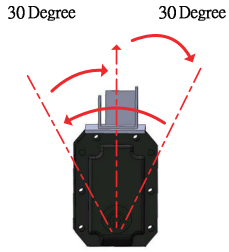

Fig. 12. The oscillation of 30 degree.

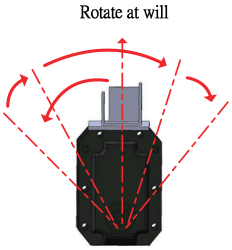

Fig. 13. The rotation at will.

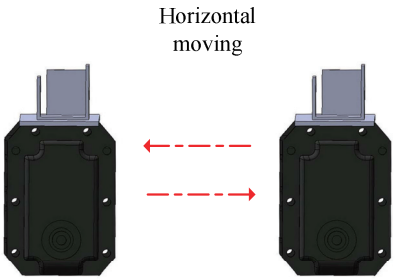

Fig. 14. The horizontal translation.

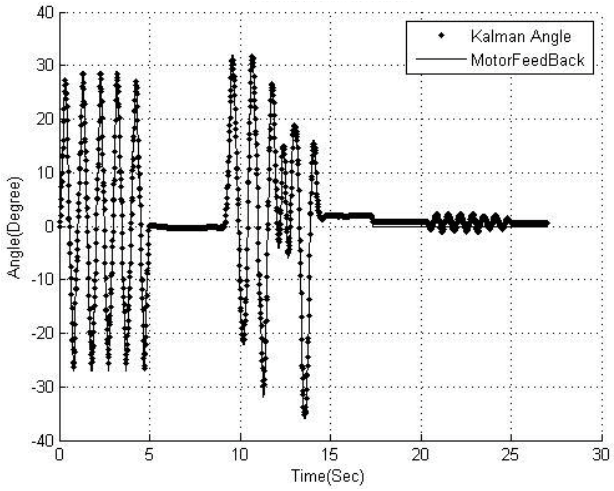

Fig. 15. The responses of three tests.

IV. Adjustment of HR for Dynamic Balance

The proposed HR without the DOF of the head is 21 DOF, whose motor ID are shown in Fig. 16. The small humanoid robot motor angle data are created by the human-machine interface. In this paper, the continuous movement of the stepping over an obstacle split in 14 single step movements as shown in Fig. 17.

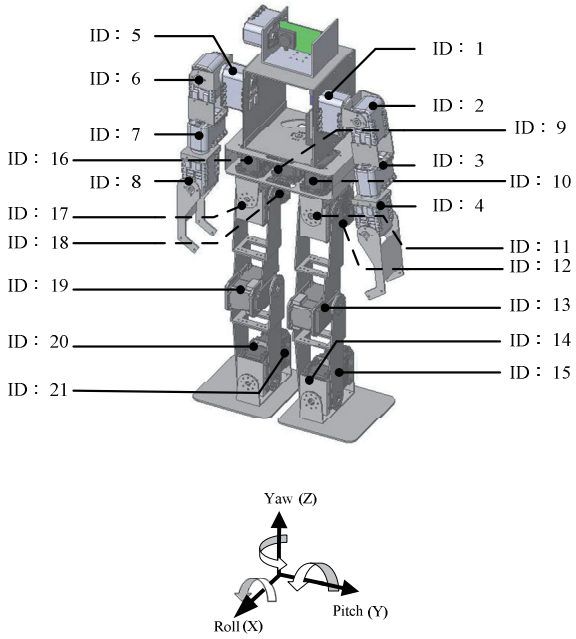

Fig. 16. The motor ID's and the definition of axes.

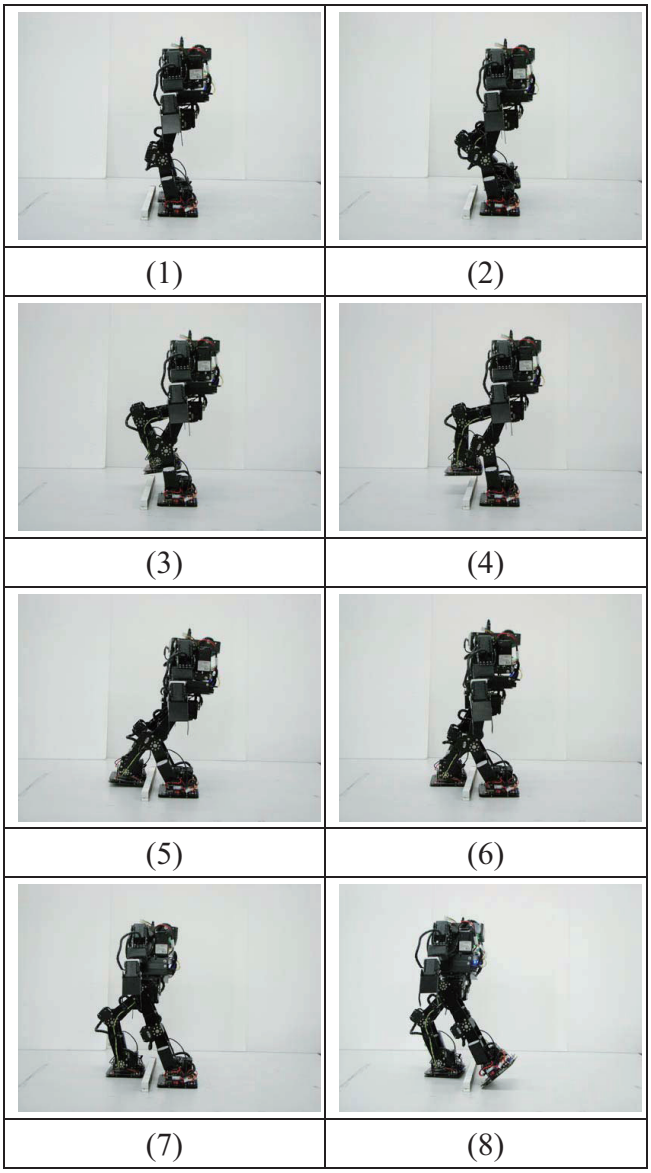

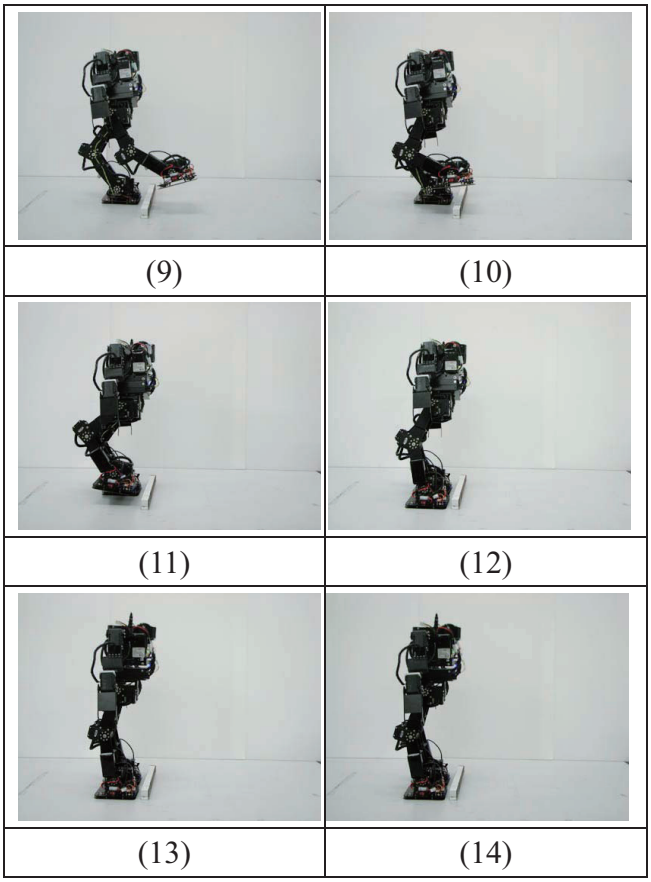

Fig. 17. Experimental result of the stepping over an obstacle.

The small humanoid robot based on the mechanism and the motor design, the movements of the forward-backward and the rightward-leftward for the proposed HR are divided into about those pitch-axis and roll-axis. Hence, the individual balance adjustments at pitch and roll axes during the double support phase (DSP) and the single support phase (SSP) are designed. In double support phase both legs hip joints and ankle joints are adjusted. Fig. 18 is the initial standing posture of the DSP. On the other hand, Fig. 19(a) depicts the backward adjustment during the DSP, which adjusts the hip joint and ankle joint to let the upper trunk of HR move backward. Similarly, Fig. 19(b) depicts the forward adjustment during DSP, whose adjustment is opposite to the direction of Fig. 19(a). When the HR is SSP, the hip joint (i.e., the motor ID 11 or 17), knee joint (i.e., the motor ID 13 or 19) and the ankle joint (i.e., the motor ID 14 or 20) of the supported leg are adjusted. Fig. 20 and Fig. 21 respectively present the back view and side view of the standing HR during SSP. Similarly, Fig. 22 and Fig. 23 respectively present the back view and side view of the rightward and leftward adjustments of the HR during SSP.

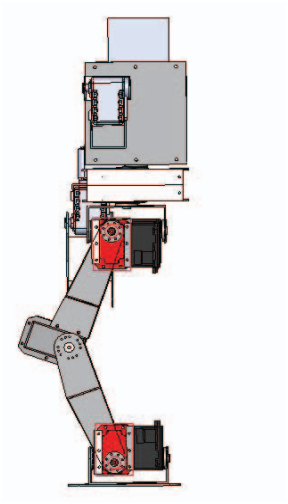

Fig. 18. The posture of initial standing during DSP.

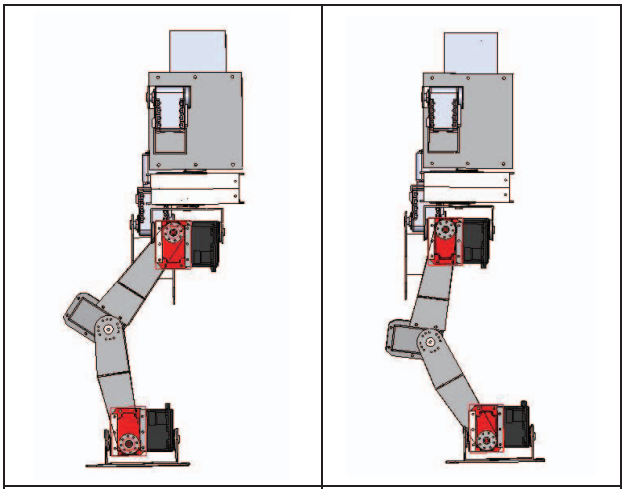

Fig. 19. The adjustments of HR forward-backward moving during DSP.

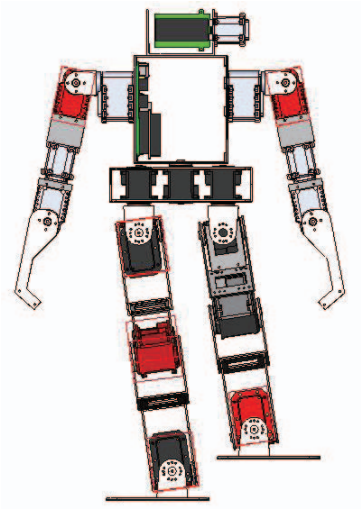

Fig. 20. The back view of the standing HR during SSP.

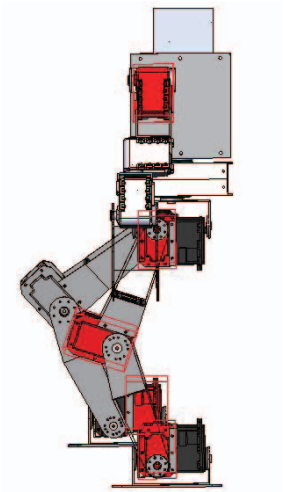

Fig. 21. The side view of the standing HR during SSP.

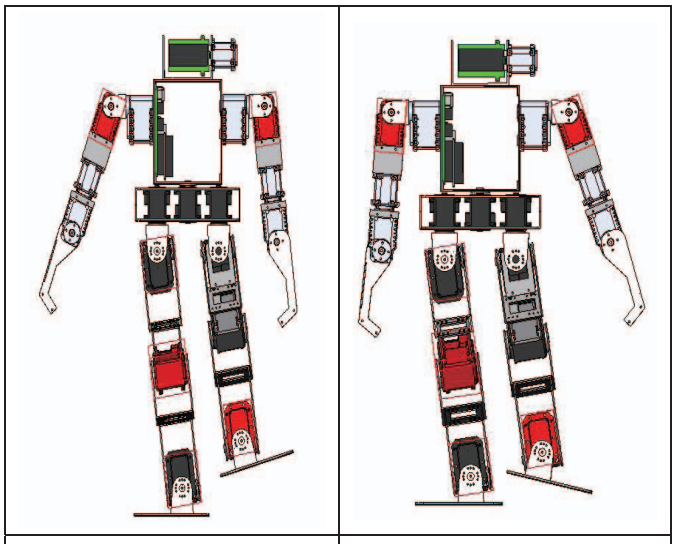

(a)rightward adjustment (b) leftward adjustment

Fig. 22. The back views of the rightward and leftward adjustments of the HR during SSP.

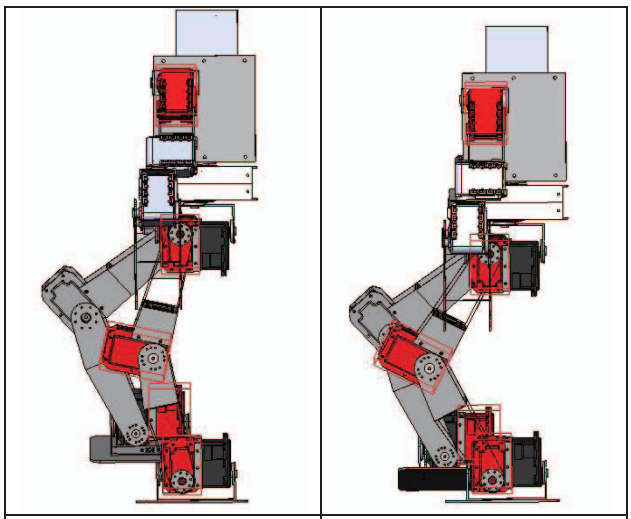

(a)backward adjustment (b) forward adjustment

Fig. 23. The side views of the rightward and leftward adjustments of the HR during SSP.

V. Dynamic Balance Using Fuzzy Decentralized Control

Based on a stable operation of the stepping over an obstacle, the corresponding posture of the HR via the gyro and accelerometer, and the COP of either SSP or DSP via two sets of the pressure sensors, are recorded. According to these two signals, two reference inputs with two DOF are planned for the balance control of the HR. Then the errors between the posture and the planned posture and between the COP and the planned COP for either SSP or DSP are applied to the proposed fuzzy decentralized balance control (FDBC) to ensure the dynamic balance of the HR during it steps over an obstacle. The reason to use the FDBC is that the dynamics of the HR is highly nonlinear and coupled, and that the dynamic balance control possesses an unstable feature. The dynamic balance must adjust immediately without causing an extra disturbance or vibration. In the beginning, the dynamics of the HR is assumed to be as follows [19]:

$$A(\theta)\ddot{\theta}(t) + B(\theta,\dot{\theta}) + C(\theta) + \Phi(\theta,\dot{\theta},t) = DU(t) \qquad (8)$$

where $\theta(t) \in \Re^8$ is the angle of the HR, $A(\theta) \in \Re^{8\times 8}$ denotes a positive definite inertia matrix, $B(\theta,\dot{\theta}) \in \Re^8$ the centrifugal and Coriolis torques, $C(\theta) \in \Re^8$ the gravitational torque, $\Phi(\theta,\dot{\theta},t)$ the nonlinear time-varying uncertainties, $D \in \Re^{8\times 8}$ the control gain, and $U(t) \in \Re^8$ is the control torque.

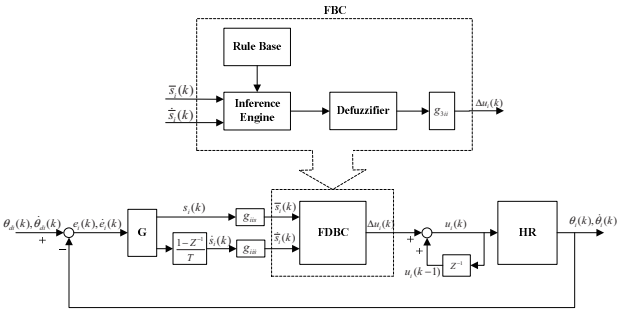

Fig.24. Block diagram of fuzzy decentralized balance control of the HR.

It is also assumed that the dynamics of (8) is unknown. However, the upper bound for the function (8) is assumed known. The FDBC includes six parallel FBCs with the switching surface:

$$S(t) = GE(t),\ G = \begin{bmatrix} G_1 & G_2 \end{bmatrix},\ E(t) = \begin{bmatrix} E_1^T(t) & E_2^T(t) \end{bmatrix}^T. \qquad (9)$$

Here $S(t) \in \Re^8$, $G_j = diag(g_{jii}) > 0 \in \Re^{6\times 6}$, $i, j = 1,2,...,8$ are the coefficients of switching surface,

$$E_1(t) = \theta_r(t) - \theta(t),\ E_2(t) = \dot{E}_1(t) \qquad (10)$$

where $E_1(t) = \begin{bmatrix} e_1(t) & e_2(t) \end{bmatrix}^T$, $\theta_r(t) \in \Re^8$ is a reference command, and $E_2(t) = \begin{bmatrix} e_3(t) & e_4(t) \end{bmatrix}^T$. The selection of G_1 and G_2 is to ensure a stable switching surface with appropriate dynamics. The FDBC is designed as

$$U(t) = G_3\overline{U}(t) = G_3\left[GE(t) + \Delta\mathrm{sgn}(GE)\right] = G_3\left[S(t) + \Delta\mathrm{sgn}(S)\right] \quad (11)$$

where $G_3 = diag(g_{3ii}) > 0 \in \Re^{8\times 8}$ is the output scaling factor, $\overline{U}(t)$ is the fuzzy variable of $U(t)$, and $\Delta = diag(\delta_{ii}) > 0 \in \Re^{8\times 8}$.

The fuzzy logic of the *ith* subsystem performs a mapping from $\Gamma_i \in \Re^2$ to $\Re$. There are l fuzzy control rules and the superscript k denotes the *kth* fuzzy rule:

$$\text{IF } \overline{s}_i(t) \text{ is } M_{1_i}^k \text{ and } \dot{\overline{s}}_i(t) \text{ is } M_{2_i}^k, \text{ THEN } \overline{u}_i(t) \text{ is } N_i^k \quad (12)$$

where $\gamma_i(t) = \left[\overline{s}_i(t) \quad \dot{\overline{s}}_i(t)\right]^T \in \Gamma_i \subset \Re^2$ and $\overline{u}_i(t) \in V_i \subset \Re$ are respectively the input and output of the fuzzy logic subsystem i; $M_{j_i}^k$ (where $i = 1,2,...,8$, $j = 1,2$, and $k = 1,2,...,l$) and N_i^k are labels of sets in Γ_i and V_i respectively. The output and input variables of the fuzzy control rule (10) are defined as $\overline{u}_i(t) = u_i(t)/g_{3ii}$, $\overline{s}_i(t) = g_{iis}s_i(t)$, and $\dot{\overline{s}}_i(t) = g_{iis}\dot{s}_i(t)$, where $\overline{u}_i(t)$, $\overline{s}_i(t)$ and $\dot{\overline{s}}_i(t) \in [-1,1]$. The corresponding fuzzy variables (e.g., $\overline{s}_i, \dot{\overline{s}}_i$ and $\overline{u}_i(t), i = 1,2,...,8$) are quantized into seven qualitative variables (i.e., $l = 7$) with triangular membership functions. The corresponding five control parameters $g_{1ii}, g_{2ii}, g_{sii}$, $g_{\dot{s}ii}$ and g_{3ii} of subsystem i are discussed in [19].

VI. Experiment Results and Discussions

To make the standardization of an added disturbance, a swing hammer shown in Fig. 25 is applied to punch the HR. The weight and the swing arm of the hammer is about 650 gram and 10 centimeter, respectively. The hammer is released from 60 degree with respect to the horizontal axis and then punches the HR. Simultaneously, the responses of angular position and angular velocity are recorded. The compared responses of the angular position without and with compensation are respectively shown in Fig. 26. Similarly, the compared responses of the angular velocity without and with compensation are respectively shown in Fig. 27. It can be seen that the response of the angular position without compensation oscillates longer and more violent than that with compensation. Similarly, the comparison of the angular velocity between without compensation and with compensation is obtained.

Based on the compensations for the SSP and DSP in the pitching and rolling axes, the dynamic balance of the HR as it is stepping over an obstacle is in progress.

Fig. 25. The standard disturbance maker.

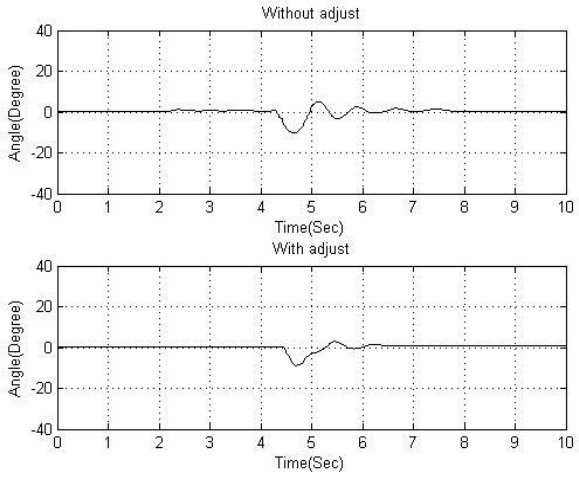

Fig. 26 The responses of angular position without and with compensation.

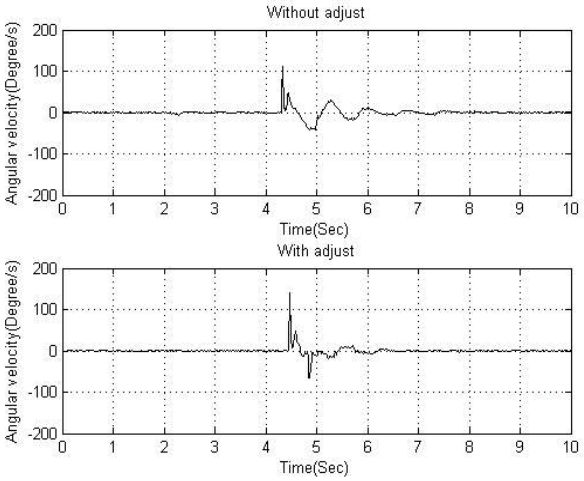

Fig. 27. The response of angular velocity without and with compensation.

VII. Conclusions

In this paper, a humanoid robot system with the consideration of dynamical balance by the feedback signals of two single-axis gyros and a three-axis

accelerometer is developed. The measured error caused by sensor's characteristic was reduced by the use of Kalman filter. To reduce the total time for capturing these feedback signals, a NIOS processor with FPGA circuit is designed. The ability of parallel processing can relax the computation loading of the main system which contains motion control and fuzzy decentralized dynamic balance control. An HMI is developed to manipulate the whole operation of an HR without the requirement of inverse kinematics. In this situation, the operation of an HR becomes easily and friendly. Subsequently, the discrete reference inputs for the dynamic balance are achieved from a stable operation of an HR for a specific task. Based on the stable planned trajectory, the fuzzy decentralized control using the feedback signals from gyros and accelerometer is applied to accomplish the desired dynamic balance as the HR is in the presence of disturbance (or unbalance), which is simulated by disturbance maker. The corresponding comparisons of angular position and angular velocity between without compensation and with compensation confirm the usefulness of the proposed methodology.

References

[1] K. Loffler, M. Gienger, F. Pfeiffer and H. Ulbrich, "Sensors and control concept of a biped robot," *IEEE Trans. Ind. Electron.*, vol. 51, no. 5, pp.972-980, Oct. 2004.

[2] Q. Huang and Y. Nakamura, "Sensory reflex control for humanoid walking," *IEEE Trans. Robotics,* vol. 21, no. 5, pp. 977-984, Oct. 2005.

[3] Y. Guan, E. S. Neo, K. Yokoi and K. Tanie, "Stepping over obstacles with humanoid robots," *IEEE Trans. Robotics*, vol. 22, no. 5, pp. 958-973, Oct. 2006.

[4] K. Harada, S. Kajita, F. Kanehiro, K. Fujiwara, K. Kaneko, K. Yokoi and H. Hirukawa, "Real-time planning of humanoid robot's gait for force-controlled manipulation," *IEEE/ASME Trans. Mechatron.*, vol. 12, no. 1, pp. 53-62, Feb., 2007.

[5] E. S. Neo, K. Yokoi, S. Kajita and K. Tanie, "Whole-body motion generation integrating operator's intention and robot's autonomy in controlling humanoid robots," *IEEE Trans. Robotics*, vol. 23, no. 4, pp.763-775, Aug. 2007.

[6] D. Xu, Y. F. Li, M. Tan and Y. Shen, "A new active visual for humanoid robots," *IEEE Trans. Syst. Man & Cyber., Part B*, vol. 38, no. 2, pp. 320-330, Apr. 2008.

[7] G. Arechavaleta, J. P. Laumond, H. Hicheur, and A. Berthoz, ''An optimality principle governing human walking,'' *IEEE Trans. Robotics*, vol. 24, no. 1, pp. 5-14, Feb. 2008.

[8] L. Montesano, M. Lopes, A. Bernardino, and Jos´e Santos-Victor, ''Learning object affordances: from sensory–motor coordination to imitation,'' *IEEE Trans. Robotics*, vol. 24, no. 1, pp. 15-264, Feb. 2008.

[9] T. Nomura, T. Kanda, T. Suzuki, and K. Kato, ''Prediction of human behavior in human–robot interaction using psychological scales for anxiety and negative postures toward robots,'' *IEEE Trans. Robotics*, vol. 24, no. 2, pp. 442-451, Apr. 2008.

[10] C. Fu and K. Chen, ''Gait synthesis and sensory control of stair climbing for a humanoid robot,'' *IEEE Trans. Ind. Electronics,* vol. 55, no. 5, pp. 2111-2120, May 2008.

[11] T. Kanda, T. Miyashita, T. Osada, Y. Haikawa, and H. Ishiguro, ''Analysis of humanoid appearances in human–robot interaction,'' *IEEE Trans. Robotics*, vol. 24, no. 3, pp. 725-735, Jun. 2008.

[12] E. Yoshida, C. Esteves, I. Belousov, J. P. Laumond, T. Sakaguchi and K. Yokoi, ''Planning 3-D collision-free dynamic robotic motion through iterative reshaping,'' *IEEE Trans. Robotics*, vol. 24, no. 3, pp. 1186-1197, Oct. 2008.

[13] C. Chevallereau, J. W. Grizzle and C. L. Shih, "Asymptotically stable walking of a five-link underactuated 3-D bipedal robot", *IEEE Trans. Robotics*, vol. 25, no. 1, pp. 37-50, Feb. 2009.

[14] M. Armand, J. P. Huissoon, and A. E. Patla, "Stepping over obstacles during locomotion: insights from multiobjective optimization on set of input parameters," *IEEE Trans. Rehabilitation Engineering*, vol. 6, no. 1, pp. 43-52, Mar. 1998.

[15] A. R. Jarfi, Q. Huang, L. Zhang, J. Yang, Z. Wang and S. Lv, "Realization and trajectory planning for obstacle stepping over by humanoid robot BHR-2," *Proceedings of the IEEE Int. Conf. on Robotics and Biomimetics*, pp. 1384-1389, December 17-20, 2006, Kunming, China.

[16] M. Vukobratovi and B. Borovac, "Zero-moment point — Thirty five years of its life," *International Journal of Humanoid Robotics*, vol. 1, no. 1, pp. 157–173, 2004.

[17] P. Sardain and G. Bessonne, ''Acting on a biped robot. center of pressure—Zero moment point," *IEEE Trans. Syst. Man & Cybern.—Part A*, vol. 34, no. 5, pp. 630-637, Sep. 2004.

[18] P. Sardain and G. BessonnetForces, ''Zero moment point—measurements from a human walker wearing robot feet as shoes," *IEEE Trans. Syst. Man & Cybern.—Part A*, vol. 34, no. 5, pp. 638-648, Sep. 2004.

[19] C. L. Hwang and C. Y. Shih, "A distributed active-vision network-space approach for trajectory tracking and obstacle avoidance of a wheeled robot," *IEEE Trans. Ind. Electronics,* vol. 56, no. 3, pp. 846-855, Mar. 2009.

[20] M. Wisse, D. G. E. Hobbelen and A. L. Schwab, "Adding an upper body to passive dynamic walking robots by means of a bisecting hip mechanism," *IEEE Trans. Robotics*, vol. 23, no. 1, pp.112-123, Feb. 2007.